Parameterised Electromagnetic Scattering Solutions for a Range of Incident Wave Angles

P.D. Ledger*[1], J. Peraire†, K. Morgan*, O. Hassan* & N.P. Weatherill*

*Civil and Computational Engineering Centre, University of Wales, Swansea, U.K.

†Aeronautics and Astronautics, M.I.T. Cambridge, Massachusetts, U.S.A

Abstract

This paper considers the numerical simulation of 2D electromagnetic wave scattering problems and describes the construction of a reduced–order approximation which enables the rapid prediction of the scattering width distribution for a range of incident wave directions. Associated certainty bounds ensure confidence in the results of the computed approximation. Numerical examples are included to demonstrate the performance of the proposed procedure.

1 Introduction

The simulation of electromagnetic wave scattering problems is of importance in many practical application areas where, typically, the interest lies in determining the scattering width distribution for a new design. Computational methods can provide assistance in this area, provided that the simulations allow the full problem parameter space of interest to be rapidly, and accurately, investigated. In general, the parameter space will include changes in the direction of the incident wave, changes in the wave frequency and changes in the geometry and structure of the scatterer. It should also be noted that this requirement for the rapid computation of the scattering width for a range of problem parameters also arises when the solution of inverse problems is considered [1].

The finite element method is a popular domain based approach for the solution of electromagnetic wave scattering problems, in which an approximation to the scattering width distribution may be obtained by post–processing the computed solution. With this approach, a new computation is necessary to produce the revised scattering width distribution following a change in any of the problem parameters. The implication is that the associated computational costs will be very high for a study involving a large number of parameter changes. In this paper, we present a reduced–order approximation which addresses this problem and can lead to significant reduction in the computational costs.

Reduced—order approximations operate in two stages. In an initial off–line stage, full solutions are computed for a set of specified problem parameters and the results of these computations are stored. In an on–line stage, specified outputs of interest are computed at low cost for new sets of the problem parameters. In addition, for the outputs to be of practical use, it is important that accuracy can be guaranteed. Reduced–order approximations with these properties have already been successfully applied in the area of computational aerodynamics [2, 3], while sophisticated methods for determining error bounds on the outputs produced by reduced–order approximations have also been developed [4, 5].

We aim to apply a reduced–order approximation in the area of electromagnetic wave scattering. For this initial study, we consider two dimensional wave scattering problems and we have restricted the parameter space investigation to allow only variations in the direction of the incident wave. The selected output of interest is the scattering width distribution and the implementation details describe how it can be effectively computed. To assess the accuracy of the proposed reduced–order approximation, a novel approach for obtaining certainty bounds on the computed output is described. Here certainty is assessed with respect to a full solution computed for the parameter set.

[1]Corresponding Author: Civil and Computational Engineering Centre, University of Wales Swansea, Singleton Park, Swansea SA2 8PP, Wales, U.K. Email: P.D.Ledger@swansea.ac.uk

It will be shown that these certainty bounds can be computed in the on–line stage, requiring little additional computation and providing certainty on the scattering width distributions. For the off–line stage of the approach, we achieve accurate solutions to two dimensional electromagnetic wave scattering problems by employing a Galerkin finite element method in the frequency domain, with the arbitrary order edge elements of Ainsworth and Coyle [6]. This has been shown to be an effective approach for obtaining accurate scattering width distributions, over a large frequency range, for a variety of different scatterers [7, 8].

The presentation of the work proceeds as follows: In Section 2, a brief description of the electromagnetic wave scattering problem, with a prescribed incident wave angle, is presented. Then, the weak variational formulation of the problem is described and an overview of the arbitrary order finite element discretisation is given, together with an outline of the approach employed for the calculation of the scattering width distribution. This is followed, in Section 3, by the presentation of the reduced–order approximation which will enable the rapid prediction of the scattering width distribution for new incident wave directions. The approach adopted for obtaining certainty bounds on the outputs produced by the reduced–order approximation is also described. In Section 4, we discuss the computational costs of the reduced–order approximation and the associated certainty bounds and, in Section 5, numerical examples are presented to illustrate the capability of the proposed method. Finally, some concluding remarks are given.

2 The Scattering Problem for a Prescribed Incident Wave Angle

2.1 Problem Description

Our interest lies in the simulation of scattering problems, in which electromagnetic waves interact with a general scatterer. We will restrict consideration to the case where the scatterer is a perfect conductor, but the method that is proposed is readily extendable to enable the modelling of more general scatterers. It is assumed that the scatterer is surrounded by a region of free space and that waves are generated by a known source located in the far field. The unknowns for this problem are the electric and magnetic field vectors, which are expressed relative to a Cartesian coordinate system $Oxyz$ in the form $\boldsymbol{E}^t = (E_x^t, E_y^t, E_z^t)^T$ and $\boldsymbol{H}^t = (H_x^t, H_y^t, H_z^t)^T$ respectively. Here, the superscripts t and T denote the total field and the vector transpose respectively. For scattering simulations, these total fields may be decomposed, into incident and scattered components, as

$$\boldsymbol{E}^t = \boldsymbol{E}^i + \boldsymbol{E} \qquad\qquad \boldsymbol{H}^t = \boldsymbol{H}^i + \boldsymbol{H} \tag{1}$$

where the superscript i denotes the incident field and the vectors $\boldsymbol{E}$ and $\boldsymbol{H}$ are the scattered electric and magnetic fields respectively. For a frequency domain approach, where a time variation $e^{\mathrm{i}\omega t}$ is assumed, the dimensionless Maxwell curl equations in free space can be expressed in the form

$$\operatorname{curl} \boldsymbol{E} = \mathrm{i}\omega \boldsymbol{H} \qquad\qquad \operatorname{curl} \boldsymbol{H} = -\mathrm{i}\omega \boldsymbol{E} \tag{2}$$

and the Maxwell divergence equations written as

$$\operatorname{div} \boldsymbol{E} = 0 \qquad\qquad \operatorname{div} \boldsymbol{H} = 0 \tag{3}$$

In these expressions $\mathrm{i}^2 = -1$ and $\omega = 2\pi/\lambda$, where λ is the wavelength of the incident wave. The curl equations (2) may be combined to produce the reduced vector wave equation

$$\operatorname{curl}\operatorname{curl} \boldsymbol{E} - \omega^2 \boldsymbol{E} = \boldsymbol{0} \tag{4}$$

for the scattered electric field. We now restrict consideration to two–dimensional transverse electric (TE) problems, in which $\boldsymbol{E}$ and $\boldsymbol{H}$ are functions of x and y only and have the form, $\boldsymbol{E} = (E_x, E_y, 0)^T$ and $\boldsymbol{H} = (0, 0, H_z)^T$ respectively. If one was to adopt a transverse magnetic formulation (TM), then the fields would have the form $\boldsymbol{H} = (H_x, H_y, 0)^T$ and $\boldsymbol{E} = (0, 0, E_z)^T$.

2.2 Boundary Conditions

2.2.1 Perfect Magnetic Conductor (PMC)

At the surface of the PMC scatterer, the boundary conditions

$$\boldsymbol{n} \wedge \boldsymbol{H} = -\boldsymbol{n} \wedge \boldsymbol{H}^i \qquad \boldsymbol{n} \cdot \boldsymbol{E} = -\boldsymbol{n} \cdot \boldsymbol{E}^i \tag{5}$$

should be applied. The surface of the PMC is denoted by Γ_1.

2.2.2 Perfect Electrical Conductor (PEC)

At the surface of the PEC scatterer, the boundary conditions are

$$\boldsymbol{n} \wedge \boldsymbol{E} = -\boldsymbol{n} \wedge \boldsymbol{E}^i \qquad \boldsymbol{n} \cdot \boldsymbol{H} = -\boldsymbol{n} \cdot \boldsymbol{H}^i \tag{6}$$

The surface of the PEC is denoted by Γ_2. It should be noted that applying a PMC condition for a TE problem is equivalent to applying a PEC condition for a TM problem.

2.2.3 Far Field Condition

The scattered fields $\boldsymbol{E}$ and $\boldsymbol{H}$ are required to satisfy the Silver–Müller radiation conditions [9]

$$\boldsymbol{e}_r \wedge \operatorname{curl} \boldsymbol{E} - \mathrm{i}\omega \boldsymbol{E} = O(r^{-3/2}) \tag{7}$$

$$\boldsymbol{e}_r \wedge \operatorname{curl} \boldsymbol{H} - \mathrm{i}\omega \boldsymbol{H} = O(r^{-3/2}) \tag{8}$$

as $r \to \infty$, where (r, θ) are cylindrical polar coordinates and $\boldsymbol{e}_r$ denotes the unit radial vector. With a finite element solution procedure in mind, we aim to approximate this condition by truncating the free space region at a finite distance from the scatterer and then imposing an appropriate boundary condition. This may be accomplished in a variety of different ways e.g. via infinite elements [10, 9], using absorbing boundary conditions [11], applying DtN maps [12] or coupling boundary and finite element methods [13]. Here, we choose to satisfy the condition by adding an absorbing layer, denoted by Ω_p, to the truncated free space region Ω_f, as illustrated

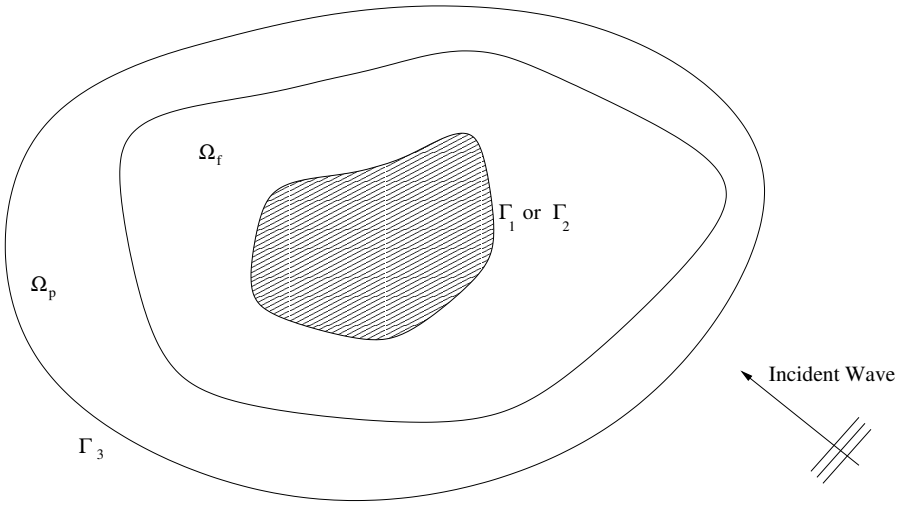

Figure 1: *The addition of Ω_p, the PML region, to the domain Ω_f*

in Figure 1. For the absorbing medium, we employ a curvilinear, anisotropic, perfectly matched layer (PML) [14, 15, 7].

2.3 Strong Statement of the Problem

It follows that a strong statement of the problem can be formulated as: find $\boldsymbol{E}$ such that

$$\left\{\begin{array}{cc} \operatorname{curl}\operatorname{curl}\boldsymbol{E}-\omega^2\boldsymbol{E}=\boldsymbol{0} & \text{in } \Omega \\ \operatorname{div}\boldsymbol{E}=0 & \text{in } \Omega \\ \boldsymbol{n}\wedge\operatorname{curl}\boldsymbol{E}=-\boldsymbol{n}\wedge\operatorname{curl}\boldsymbol{E}^i \qquad \boldsymbol{n}\cdot\boldsymbol{E}=-\boldsymbol{n}\cdot\boldsymbol{E}^i & \text{on } \Gamma_1 \\ \boldsymbol{n}\wedge\boldsymbol{E}=-\boldsymbol{n}\wedge\boldsymbol{E}^i & \text{on } \Gamma_2 \\ \boldsymbol{e}_r\wedge\operatorname{curl}\boldsymbol{E}-\mathrm{i}\omega\boldsymbol{E}=O(r^{-3/2}) & \text{as } r\to\infty \end{array}\right. . \tag{9}$$

This equation set can be shown to be equivalent to the problem description given in section 2.1 and the boundary conditions given in section 2.2 [16]. Note that the normal condition $\boldsymbol{n}\cdot\boldsymbol{H}$ associated with Γ_2 can be discarded because the normal condition $\boldsymbol{n}\cdot\boldsymbol{E}=-\boldsymbol{n}\cdot\boldsymbol{E}^i$ on Γ_1 implies that $\boldsymbol{n}\cdot\boldsymbol{H}=-\boldsymbol{n}\cdot\boldsymbol{H}^i$ on Γ_2.

2.4 Weak Variational Statement and Discretisation

A weak variational formulation of the scattering problem given in equation (9) may now be expressed as [7, 8]: find $\boldsymbol{E}\in X^D$, such that

$$\mathcal{A}(\boldsymbol{E},\boldsymbol{W})=\ell(\boldsymbol{W}) \qquad\qquad \forall\boldsymbol{W}\in X \tag{10}$$

where the spaces X^D and X are defined by

$$X^D=\{\boldsymbol{v}\,|\,\boldsymbol{v}\in\mathcal{H}(\operatorname{curl};\Omega);\ \boldsymbol{n}\wedge\boldsymbol{v}=-\boldsymbol{n}\wedge\boldsymbol{E}^i \text{ on } \Gamma_2;\ \boldsymbol{n}\wedge\boldsymbol{v}=\boldsymbol{0} \text{ on } \Gamma_3\} \tag{11}$$

$$X=\{\boldsymbol{v}\,|\,\boldsymbol{v}\in\mathcal{H}(\operatorname{curl};\Omega);\ \boldsymbol{n}\wedge\boldsymbol{v}=\boldsymbol{0} \text{ on } \Gamma_2;\ \boldsymbol{n}\wedge\boldsymbol{v}=\boldsymbol{0} \text{ on } \Gamma_3\} \tag{12}$$

and the operator $\mathcal{A}$ is defined by

$$\mathcal{A}(\boldsymbol{E},\boldsymbol{W})=a(\boldsymbol{E},\boldsymbol{W})-\omega^2 m(\boldsymbol{E},\boldsymbol{W}) \tag{13}$$

The bilinear forms employed here are defined by

$$a(\boldsymbol{E},\boldsymbol{W})=\int_{\Omega_f+\Omega_p}\boldsymbol{\Lambda}_1^{-1}\operatorname{curl}\boldsymbol{E}\cdot\operatorname{curl}\overline{\boldsymbol{W}}\,\mathrm{d}\Omega \qquad\qquad m(\boldsymbol{E},\boldsymbol{W})=\int_{\Omega_f+\Omega_p}\boldsymbol{\Lambda}_2\boldsymbol{E}\cdot\overline{\boldsymbol{W}}\mathrm{d}\Omega \tag{14}$$

and the linear form is given by

$$\ell(\boldsymbol{W})=\int_{\Gamma_1}\left(\boldsymbol{n}\wedge\boldsymbol{\Lambda}_1^{-1}\operatorname{curl}\boldsymbol{E}^i\right)\cdot\overline{\boldsymbol{W}}\,\mathrm{d}\Gamma \tag{15}$$

In these expressions, $\boldsymbol{\Lambda}_1$ and $\boldsymbol{\Lambda}_2$ represent complex tensors of position in Ω_p and are equal to the identity tensor in Ω_f [7], while an overbar denotes the complex conjugate. One might expect that a Lagrange multiplier term should be included in equation (10) to enforce the zero divergence condition. However, it can be shown that, for scattering problems with a prescribed non-zero ω, the Lagrange multiplier turns out to be equal to zero and therefore can be omitted [8]. As the normal boundary condition $\boldsymbol{n}\cdot\boldsymbol{E}=-\boldsymbol{n}\cdot\boldsymbol{E}^i$ on Γ_1 is associated with the divergence condition it does not appear in the variational statement (10).

An approximate solution $\boldsymbol{E}_H\in X_H^D\subset X^D$ to the problem expressed by the variational statement of equation (10) is obtained by employing the Galerkin procedure. Initially, the domain $\Omega_f+\Omega_p$ is discretised using an unstructured assembly of triangular and quadrilateral elements. Then, the scattered field is approximated, to a degree p, as [6]

$$\hat{\boldsymbol{E}}_H=\sum_{i=1}^{4}\sum_{j=0}^{p}e_j^i\hat{\boldsymbol{\phi}}_j^{\,i}+\sum_{j=0}^{p}\sum_{k=1}^{p}e_{j,k}^{I_\xi}\hat{\boldsymbol{\phi}}_{j,k}^{I_\xi}+\sum_{j=0}^{p}\sum_{k=1}^{p}e_{j,k}^{I_\eta}\hat{\boldsymbol{\phi}}_{j,k}^{I_\eta} \tag{16}$$

over a master quadrilateral element and as

$$\hat{\boldsymbol{E}}_H = \sum_{i=1}^{3}\sum_{j=0}^{p} e_j^i \hat{\boldsymbol{\phi}}_j^i + \sum_{i=1}^{3}\sum_{j=0}^{p-2} e_{i,j}^{PI}\hat{\boldsymbol{\phi}}_{i,j}^{PI} + \underbrace{\sum_{j=0}^{p-3}\sum_{k=0}^{p-3}}_{j+k\leq p-3} e_{j,k}^{GI_\xi}\hat{\boldsymbol{\phi}}_{j,k}^{GI_\xi} + \underbrace{\sum_{j=0}^{p-3}\sum_{k=0}^{p-3}}_{j+k\leq p-3} e_{j,k}^{GI_\eta}\hat{\boldsymbol{\phi}}_{j,k}^{GI_\eta} \tag{17}$$

over a master triangular element. The vectors $\hat{\boldsymbol{\phi}}$, expressed relative to a master element coordinate system, denote the hierarchic edge element basis functions, while the scalars e are the unknown coefficients. These scalar coefficients are related to weighted moments of the tangential component of the field and continuity of these coefficients is enforced on inter–element edges. This results in a scheme which has continuous tangential components between elements, whilst allowing for discontinuous normal components.

The basis functions can be generated numerically through recursive relations [6]. Element integrals can be evaluated by employing a covariant mapping [17] and Gauss quadrature [7]. Following this approach, the Galerkin approximation is obtained as the solution of a discrete problem which can be expressed as: find $\boldsymbol{E}_H \in X_H^D$ such that

$$\mathcal{A}(\boldsymbol{E}_H, \boldsymbol{W}) = \ell(\boldsymbol{W}) \qquad\qquad \forall \boldsymbol{W} \in X_H \subset X \tag{18}$$

The complex linear equation system

$$\mathbf{A}\boldsymbol{E}^H = \boldsymbol{L} \tag{19}$$

which results from equation (18) is solved using a LINPACK banded solver. Here, we use the notation $\boldsymbol{E}^H$ to denote the vector of unknown coefficients associated with a pth order discretisation.

2.5 Scattering Width Evaluation

The computed scattering width distribution $\hat{\sigma}(\boldsymbol{E}_H;\phi)$ is a function of the finite element solution $\boldsymbol{E}_H$ and the far field viewing angle ϕ. To evaluate the scattering width distribution, the form of the solution on a collection surface Γ_c, which totally encloses the scatterer, is determined. It is convenient to express the scattering width distribution in the form [18]

$$\hat{\sigma}(\boldsymbol{E}_H;\phi) = \mathcal{L}^{\mathcal{O}}(\boldsymbol{E}_H;\phi)\overline{\mathcal{L}^{\mathcal{O}}(\boldsymbol{E}_H;\phi)} \tag{20}$$

where

$$\mathcal{L}^{\mathcal{O}}(\boldsymbol{E}_H;\phi) = \int_{\Gamma_c} (\boldsymbol{n}\wedge\boldsymbol{E}_H\cdot\boldsymbol{V})\,\mathrm{d}\Gamma + \sum\int_k \left(\omega^2\boldsymbol{E}_H\cdot\boldsymbol{Y}_H - \operatorname{curl}\boldsymbol{E}_H\cdot\operatorname{curl}\boldsymbol{Y}_H\right)\mathrm{d}\Omega \tag{21}$$

Here, the summation extends over all elements $k\in\Omega$, such that $\partial k\cup\Gamma_c\neq\emptyset$ and

$$\boldsymbol{V} = -[0,0,1]^T\exp\left\{\mathrm{i}\omega\left(x'\cos\phi + y'\sin\phi\right)\right\} \tag{22}$$

$$\boldsymbol{Y} = \frac{1}{\mathrm{i}\omega}[\sin\phi,-\cos\phi,0]^T\exp\left\{\mathrm{i}\omega\left(x'\cos\phi + y'\sin\phi\right)\right\} \tag{23}$$

The quantity $\boldsymbol{Y}_H$ is the finite element interpolant of $\boldsymbol{Y}$. It should be noted that equation (21) follows from adopting the approach of Monk and co–workers [19, 20, 21], who suggested using an area integral approach to evaluate the flux term which appears in the basic scattering width expression. The scattering width distribution is generally displayed in decibels and, in this case, it is the quantity

$$\sigma = 10\log_{10}\left(\frac{\omega}{4}\hat{\sigma}(\boldsymbol{E}_H;\phi)\right) \tag{24}$$

that is plotted against the viewing angle ϕ.

3 Reduced Order Approximation

3.1 Computing the Reduced Order Approximation

Consider now the development of a reduced–order approximation for the prediction of the scattering width distribution for an electromagnetic scattering problem. We take incident waves of the form

$$\boldsymbol{E}^i = \begin{bmatrix} -\sin\theta \\ \cos\theta \\ 0 \end{bmatrix} \exp\{\mathrm{i}\omega(x\cos\theta + y\sin\theta)\} \tag{25}$$

where θ is the angle between the direction of propagation of the incident wave and the x axis. We return to the standard Galerkin statement of equation (18), but now expressed in the form [4]: find $\boldsymbol{E}_H(\theta) \in X_H^D$ such that

$$\mathcal{A}(\boldsymbol{E}_H(\theta), \boldsymbol{W}) = \ell(\boldsymbol{W}; \theta) \qquad \forall \boldsymbol{W} \in X_H \tag{26}$$

for a given incident wave direction, θ. Our goal is to develop a reduced–order approximation for a parameterised solution $\boldsymbol{E}_H(\theta)$. The computed output is selected to be $s_H(\theta;\phi) \in \mathbb{C}$, where

$$s_H(\theta, \phi) = \mathcal{L}^{\mathcal{O}}(\boldsymbol{E}_H(\theta); \phi) \tag{27}$$

and $\mathcal{L}^{\mathcal{O}}$ is defined in equation (21). We introduce the associated adjoint solution, $\boldsymbol{\Psi}_H(\phi) \in X_H$, which is defined to satisfy the requirement

$$\mathcal{A}(\boldsymbol{W}, \boldsymbol{\Psi}_H(\phi)) = -\mathcal{L}^{\mathcal{O}}(\boldsymbol{W}; \phi) \qquad \forall \boldsymbol{W} \in X_H \tag{28}$$

Note that here we prefer to use $\mathcal{L}^{\mathcal{O}}(\boldsymbol{W};\phi)$ for the adjoint computation, rather than the linearised form of $\hat{\sigma}$ which we previously proposed when evaluating a–posteriori error bounds on the scattering width [18]. The reasons for this choice are

1. Use of the the linearised form of $\hat{\sigma}$ results in asymptotic bounds, which although applicable in the case of evaluating a–posteriori error bounds is not in the case of this reduced order model. Indeed, if the linearised form of $\hat{\sigma}$ is employed for this reduced order model we would lose the guarantee of being able to prove that the bounds we obtain are strict;

2. Use of the linearised form of $\hat{\sigma}$ as the output adjoint for a reduced–order approximation would, in the approach to be followed, necessitate the calculation of a large number of additional adjoint solutions, since the linearised adjoint then depends on the solution $\boldsymbol{E}_H$.

The discrete adjoint problem, given in equation (28), may be written in matrix notation as

$$\mathbf{A}^T \boldsymbol{\Psi}^H = -\boldsymbol{g} \tag{29}$$

where $\boldsymbol{g}$ is the right hand vector which results from the linear form $\mathcal{L}^{\mathcal{O}}(\boldsymbol{W};\phi)$.

To construct reduced–order spaces, we adopt a parameter set $\{\theta_1, \cdots, \theta_{N_\theta}\}$ of incident wave angles and a parameter set $\{\phi_1, \cdots, \phi_{N_\phi}\}$ of viewing angles of the scattering width. Corresponding solutions $\boldsymbol{E}_H(\theta_1), \cdots, \boldsymbol{E}_H(\theta_{N_\theta})$ and adjoints $\boldsymbol{\Psi}(\phi_1), \cdots, \boldsymbol{\Psi}(\phi_{N_\phi})$ are computed, and the spaces

$$W_{N_\theta} = \mathrm{span}\{\boldsymbol{E}_H(\theta_i); i = 1, \cdots, N_\theta\} \qquad W_{N_\phi} = \mathrm{span}\{\boldsymbol{\Psi}_H(\phi_i); i = 1, \cdots, N_\phi\} \tag{30}$$

are defined. If we are presented with a new incident angle, θ, the approach is then to look for $\tilde{\boldsymbol{E}}_H(\theta) \in W_{N_\theta} \subset X_H^D$ such that

$$\mathcal{A}(\tilde{\boldsymbol{E}}_H, \boldsymbol{W}) = \ell(\boldsymbol{W}; \theta) \qquad \forall \boldsymbol{W} \in W_{N_\theta} \tag{31}$$

For this angle of incidence, we compute $\tilde{\boldsymbol{\Psi}}_H(\phi) \in W_{N_\phi} \subset X_H$, for a given ϕ, such that

$$\mathcal{A}(\boldsymbol{W}, \tilde{\boldsymbol{\Psi}}_H) = -\mathcal{L}^{\mathcal{O}}(\boldsymbol{W}; \phi) \qquad \forall \boldsymbol{W} \in W_{N_\phi} \tag{32}$$

Here, $\tilde{\boldsymbol{E}}_H$ denotes a reduced–order approximation to $\boldsymbol{E}_H(\theta)$ and $\tilde{\boldsymbol{\Psi}}_H$ is a reduced–order approximation to $\boldsymbol{\Psi}_H(\phi)$.

With the viewing angle, ϕ, and the incident wave direction, θ, specified, equation (27) may be expressed as

$$s_H(\theta,\phi) = \mathcal{L}^{\mathcal{O}}(\boldsymbol{E}_H(\theta);\phi) = \mathcal{L}^{\mathcal{O}}(\tilde{\boldsymbol{E}}_H;\phi) + \mathcal{L}^{\mathcal{O}}(\boldsymbol{E}_H(\theta) - \tilde{\boldsymbol{E}}_H;\phi) \tag{33}$$

since $\mathcal{L}^{\mathcal{O}}(\boldsymbol{E};\phi)$ is linear in $\boldsymbol{E}$. Then, using equations (28) and (26), it follows that we can write

$$s_H(\theta,\phi) = \tilde{s}_H(\theta,\phi) + r(\theta,\phi) \tag{34}$$

Here

$$\tilde{s}_H(\theta,\phi) = \mathcal{L}^{\mathcal{O}}(\tilde{\boldsymbol{E}}_H;\phi) - \Big[\ell(\tilde{\boldsymbol{\Psi}}_H) - \mathcal{A}(\tilde{\boldsymbol{E}}_H,\tilde{\boldsymbol{\Psi}}_H)\Big] \tag{35}$$

is computable from the known data, while the term

$$r(\theta,\phi) = \mathcal{A}(\boldsymbol{E}_H(\theta) - \tilde{\boldsymbol{E}}_H, \boldsymbol{\Psi}_H(\phi) - \tilde{\boldsymbol{\Psi}}_H) \tag{36}$$

is not computable without prior knowledge of $\boldsymbol{E}_H(\theta)$ or $\boldsymbol{\Psi}_H(\phi)$. Although this term is not computable, we will see below that it may be bounded, and this enables us to deduce the magnitude of the error made when we employ $\tilde{s}_H$ as a reduced order approximation to s_H. We note that this approach differs to the direct method of employing $\mathcal{L}^{\mathcal{O}}(\tilde{\boldsymbol{E}}_H;\phi)$ as the reduced order approximation to s_H and results in a much improved approximation.

To summarise this process, the steps involved in the off–line and on–line stages of the reduced–order approximation procedure are presented in algorithmic form in Table 1.

3.2 Bounding the Error in the Reduced Order Approximation

Certainty bounds may be constructed for the reduced–order approximation to the output, with the bounds being measured with respect to the output given by the finite element solution. From equations (34)–(36), it can be seen that the error in the reduced order approximation may be written as

$$s_H - \tilde{s}_H = r(\theta,\phi) = \mathcal{A}(e,\epsilon) \tag{37}$$

where

$$e = \boldsymbol{E}_H - \tilde{\boldsymbol{E}}_H \qquad\qquad \epsilon = \boldsymbol{\Psi}_H - \tilde{\boldsymbol{\Psi}}_H \tag{38}$$

Given the reduced order approximations $\tilde{\boldsymbol{E}}_H$ and $\tilde{\boldsymbol{\Psi}}_H$, we define residuals $R^U(\boldsymbol{W}) : X_H \to \mathbb{R}$ and $R^\Psi(\boldsymbol{W}) : X_H \to \mathbb{R}$ according to

$$R^U(\boldsymbol{W}) = \ell(\boldsymbol{W}) - \mathcal{A}(\tilde{\boldsymbol{E}}_H,\boldsymbol{W}) \qquad\qquad R^\Psi(\boldsymbol{W}) = -\mathcal{L}^{\mathcal{O}}(\boldsymbol{W}) - \mathcal{A}(\boldsymbol{W},\tilde{\boldsymbol{\Psi}}_H) \tag{39}$$

and we note that

$$R^U(\boldsymbol{\epsilon}) = R^\Psi(\boldsymbol{e}) = \mathcal{A}(\boldsymbol{e},\boldsymbol{\epsilon}) \tag{40}$$

For the space X_H, we introduce a norm $\|\cdot\|_*$, defined by

$$\|\boldsymbol{W}\|_* = n(\boldsymbol{W},\boldsymbol{W}) \geq 0 \tag{41}$$

where n is a coercive bilinear form and the particular choice adopted for n will be described below. For the residuals $R^U(\boldsymbol{W})$ and $R^\Psi(\boldsymbol{W})$, we also define the dual norm $\|\cdot\|_{-*}$ of $\|\cdot\|_*$ according to

$$\|R\|_{-*} = \sup_{\boldsymbol{W}\in X_H} \frac{R(\boldsymbol{W})}{\|\boldsymbol{W}\|_*} \tag{42}$$

From this dual norm definition, it follows that

$$|R(\boldsymbol{W})| \leq \|R\|_{-*}\|\boldsymbol{W}\|_* \qquad\qquad \forall\ \boldsymbol{W}\ \in\ X_H \tag{43}$$

Off–Line Stage:

Select $\{\theta_1, \cdots, \theta_{N_\theta}\}$ and $\{\phi_1, \cdots, \phi_{N_\phi}\}$

Compute the coefficents $\boldsymbol{E}_i^H$ for $i = 1, \cdots N_\theta$ by solving
$\mathbf{A}\boldsymbol{E}_i^H = \boldsymbol{L}_i$

Compute the coefficients $\boldsymbol{\Psi}_i^H$ for $i = 1, \cdots N_\phi$ by solving
$\mathbf{A}^T\boldsymbol{\Psi}_i^H = -\boldsymbol{g}_i$

On–Line Stage:

Select a new incident wave direction θ

Compute the coefficients α_i of $\tilde{\boldsymbol{E}}^H = \sum_{i=1}^{N_\theta} \alpha_i \boldsymbol{E}_i^H$ by solving
$(\boldsymbol{E}_i^H)^T\mathbf{A}\tilde{\boldsymbol{E}}^H = (\boldsymbol{E}_i^H)^T\boldsymbol{L}_i \qquad i = 1, \cdot, N_\theta$

Compute the coefficents β_i of $\tilde{\boldsymbol{\Psi}}^H = \sum_{i=1}^{N_\phi} \beta_i \boldsymbol{\Psi}_i^H$ by solving
$(\boldsymbol{\Psi}_i^H)^T\mathbf{A}^T\tilde{\boldsymbol{\Psi}}^H = -(\boldsymbol{\Psi}_i^H)^T\boldsymbol{g}_i \qquad i = 1, \cdots, N_\phi$

Then compute $\tilde{s}_H$ from
$\tilde{s}_H = \boldsymbol{g}^T\tilde{\boldsymbol{E}}^H - \left[\boldsymbol{L}^T\tilde{\boldsymbol{\Psi}}^H - \left(\tilde{\boldsymbol{\Psi}}^H\right)^T \mathbf{A}\tilde{\boldsymbol{E}}^H\right]$

The scattering width distribution is then given by
$\hat{\sigma} = \tilde{s}_H\overline{\tilde{s}_H}$

Table 1: *Algorithmic description of the reduced–order approximation procedure for the scattering width distribution, detailing the off–line and on–line stages*

so that, in particular, when $\boldsymbol{W} = \boldsymbol{e}$,

$$\left|R^\Psi(\boldsymbol{e})\right| \leq \|R^\Psi\|_{-*}\|\boldsymbol{e}\|_* \tag{44}$$

In order to be able to determine a computable bound for $s_H - \tilde{s}_H$, we require the existence of a discrete inf–sup parameter β that satisfies

$$\inf_{\boldsymbol{V}\in X_H} \sup_{\boldsymbol{W}\in X_H} \frac{|\mathcal{A}(\boldsymbol{V},\boldsymbol{W})|}{\|\boldsymbol{V}\|_*\|\boldsymbol{W}\|_*} \geq \beta > 0 \tag{45}$$

It should be noted that the existence of this parameter is a requirement for the original problem of equation (18) to be well–posed. Now, if we set $\boldsymbol{V} = \boldsymbol{e}$ in this equation, we may deduce that

$$\sup_{\boldsymbol{W}\in X_H} \frac{|\mathcal{A}(\boldsymbol{e},\boldsymbol{W})|}{\|\boldsymbol{W}\|_*} \geq \beta\|\boldsymbol{e}\|_* \tag{46}$$

When this result is combined with equations (40) and (42), we see immediately that

$$\|\boldsymbol{e}\|_* \leq \frac{1}{\beta}\|R^U\|_{-*} \tag{47}$$

Off–Line Stage:

Compute the minimum singular value μ_i of the matrix $\mathbf{A}$

On–Line Stage:

For a chosen wave direction θ

Compute the scattering residual
$\boldsymbol{R}^U = \boldsymbol{L} - \mathbf{A}\boldsymbol{E}^{N_\theta}$

For all ϕ compute the adjoint residual
$\boldsymbol{R}^\Psi = -\boldsymbol{g} - \mathbf{A}^T\boldsymbol{\Psi}^{N_\phi}$

and the bounds
$\Delta\hat{\sigma} = (\Delta|\tilde{s}_H|)^2 = \left(\dfrac{\|\boldsymbol{R}^\Psi\|\,\|\boldsymbol{R}^U\|}{\min\mu_i}\right)^2$

Table 2: *The algorithm for calculating bounds on the scattering width distribution given by the reduced–order approximation showing the off–line and on–line stages*

and it follows, using equation (44), that

$$s_H - \tilde{s}_H \leq \left|R^\Psi(\boldsymbol{e})\right| \leq \frac{1}{\beta}\|R^\Psi\|_{-*}\|R^U\|_{-*} \tag{48}$$

3.3 Selected Implementation

If we represent the elements of X_H in terms of the edge basis functions of equations (16) and (17), we can write

$$\boldsymbol{V} = \boldsymbol{v}^T\boldsymbol{\phi} \qquad\qquad \forall \boldsymbol{V} \in X_H \tag{49}$$

In this case, it follows that

$$\|\boldsymbol{V}\|_*^2 = \boldsymbol{v}^T\boldsymbol{N}\boldsymbol{v} \qquad\qquad \|R\|_{-*}^2 = R^T\boldsymbol{N}^{-1}R \tag{50}$$

where $\boldsymbol{N} = n(\boldsymbol{\phi},\boldsymbol{\phi})$, and the inf–sup parameter is then given, from a generalised eigenvalue problem, as

$$\beta^2 = \max_{\boldsymbol{v}} \frac{\boldsymbol{v}^T\mathbf{A}^T\boldsymbol{N}^{-1}\mathbf{A}\boldsymbol{v}}{\boldsymbol{v}^T\boldsymbol{N}\boldsymbol{v}} \tag{51}$$

Here, for computational efficiency, we choose $\boldsymbol{N}$ to be the identity matrix, in which case β becomes the minimum of the singular values μ_i of $\mathbf{A}$ and $\|\cdot\|_*$ and $\|\cdot\|_{-*}$ are vector euclidean norms. Of course, other possible choices could be adopted, but these might be computationally less advantages. In Algorithm 2, we summarise the steps required to obtain, in this fashion, the certainty bounds on outputs predicted by the reduced–order model.

4 Computational Costs

To assess the computational costs associated with the reduced–order model, it is convenient to consider the off–line and on–line stages separately.

In the off–line stage, the implementation of the reduced–order approximation requires the computation of N_θ problem solutions and N_ϕ adjoint solutions. For each case, the matrix $\mathbf{A}$

remains unaltered and only the right hand side vectors $\boldsymbol{g}$ and $\boldsymbol{L}$ change. By using a LINPACK direct solution technique which allows for multiple right hand side vectors, we are able to compute all these solutions simultaneously. In preparation for the calculation of bounds, we are required

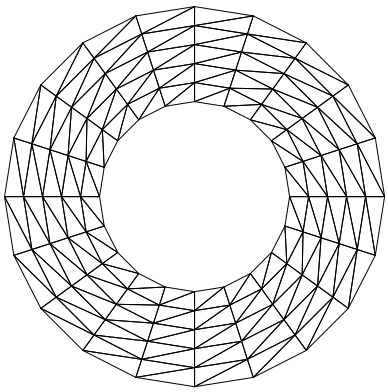

Figure 2: *Scattering by a PEC/PMC circular cylinder of diameter* $D = 2\lambda$ *showing the structured mesh of* 200 *triangular elements*

to evaluate the minimum of the singular values of the matrix $\mathbf{A}$. Although this is an expensive $\mathcal{O}(N^3)$ operation, it only has to be undertaken once for all incident wave directions.

In the on–line stage, we prescribe new incident wave directions and compute $\tilde{\boldsymbol{E}}^H$ and $\tilde{\boldsymbol{\Psi}}^H$ as linear combinations of the predetermined data given in W_{N_θ} and W_{N_ϕ}. The $N_\theta \times N_\theta$ and the $N_\phi \times N_\phi$ matrices which result from equations (31) and (32) can be precomputed to reduce the cost of computing subsequent outputs for new θ values. Inversion of the resulting system for $\tilde{\boldsymbol{E}}^H, \tilde{\boldsymbol{\Psi}}^H$ is at most, $O(\max(N_\theta^3, N_\phi^3))$ and we deduce that, for small N_θ and N_ϕ, $\tilde{s}_H$ is much less expensive to compute than s_H.

Further computational efficiencies can be obtained by storing quantities which remain unaltered during evaluation of different RCS values.

5 Numerical Examples

A number of numerical examples are now considered to demonstrate the performance of the proposed procedure. Initially, the reduced–order approximation of equation (35) is used to predict the scattering width distribution, following the algorithm shown in Table 1. Then, we demonstrate the evaluation of bounds for the scattering width distribution using equation (48) and the selected implementation, following the algorithm outlined in Table 2.

5.1 Performance of the Reduced–Order Approximation

To demonstrate the performance of the reduced–order approximation, consider initially the problem of scattering of a plane TE wave by a PMC circular cylinder of diameter $D = 2\lambda$. The computational domain is in the form of a circular annulus of inner radius λ and outer radius 2λ. This domain is discretised using a structured mesh of 200 triangular elements of polynomial order $p = 4$, as illustrated in Figure 2. For this example, off–line solutions corresponding to $N_\theta = 3$, with incident wave directions $\theta_i = \{-90, 0, 90\}$ degrees, and viewing angles $N_\phi = 18$ with $\phi_i = -180 + 20(i-1)$ degrees for $i = 1, 2, \ldots, 18$, are computed. Using these computed results, the reduced–order approximation is invoked, in the on–line stage, to predict the scattering width distributions for waves incident at angles of $\theta = \{0, 10, 20, 40, 120\}$ degrees in turn. A comparison between the resulting distributions in decibels and the distributions obtained from the full finite element solutions are shown in Figure 3. It can be observed that for the case $\theta = 0$, which corresponds to one of the primal problems, the reduced–order approximation produces results that are in exact agreement with the finite element distribution. For angles of incidence

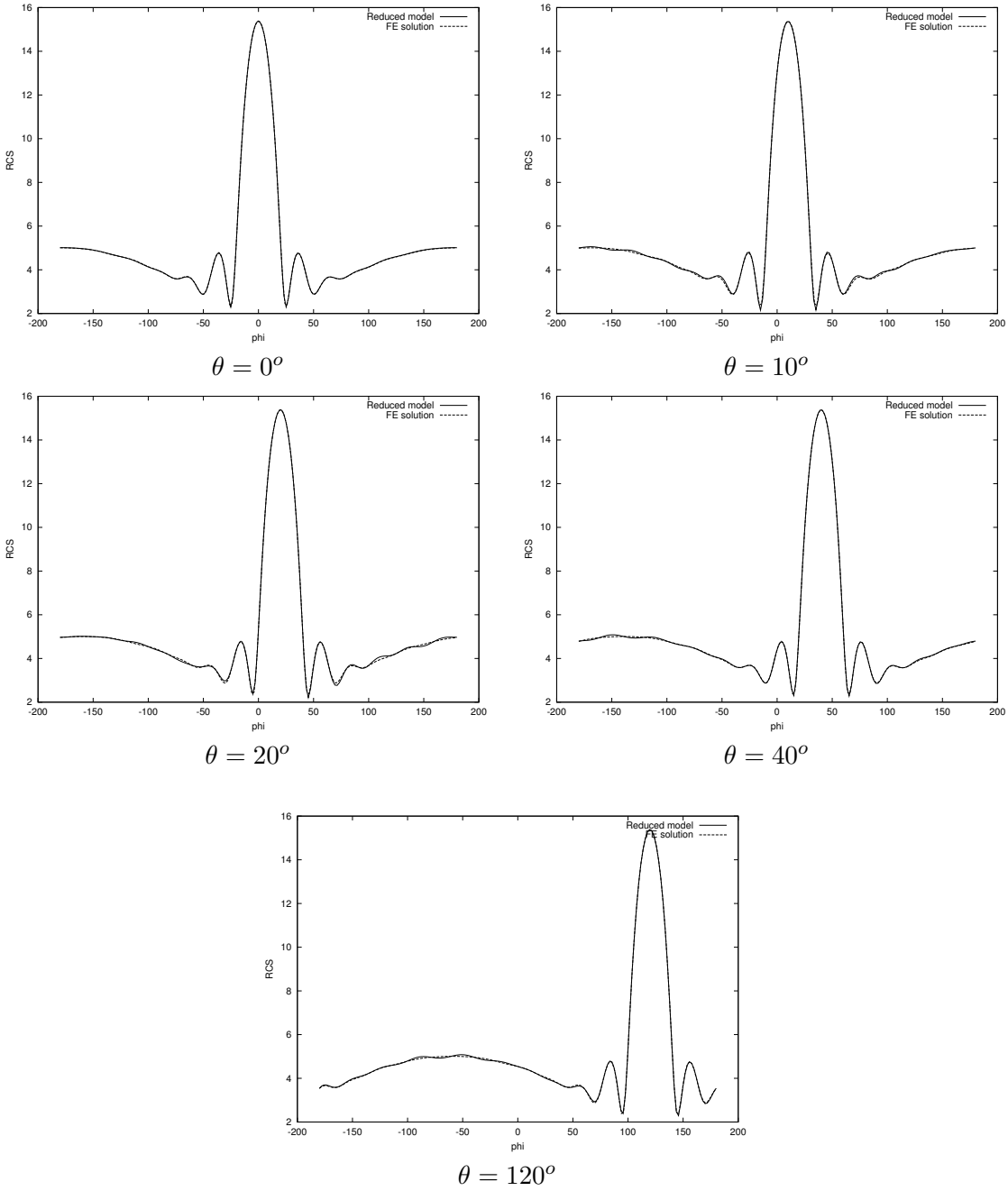

Figure 3: *Scattering of a plane TE wave by a PMC circular cylinder of diameter $D = 2\lambda$ showing a comparison between the scattering width distributions computed using the adjoint enhanced reduced–order model solution and the finite element solution, for waves incident at different angles, θ.*

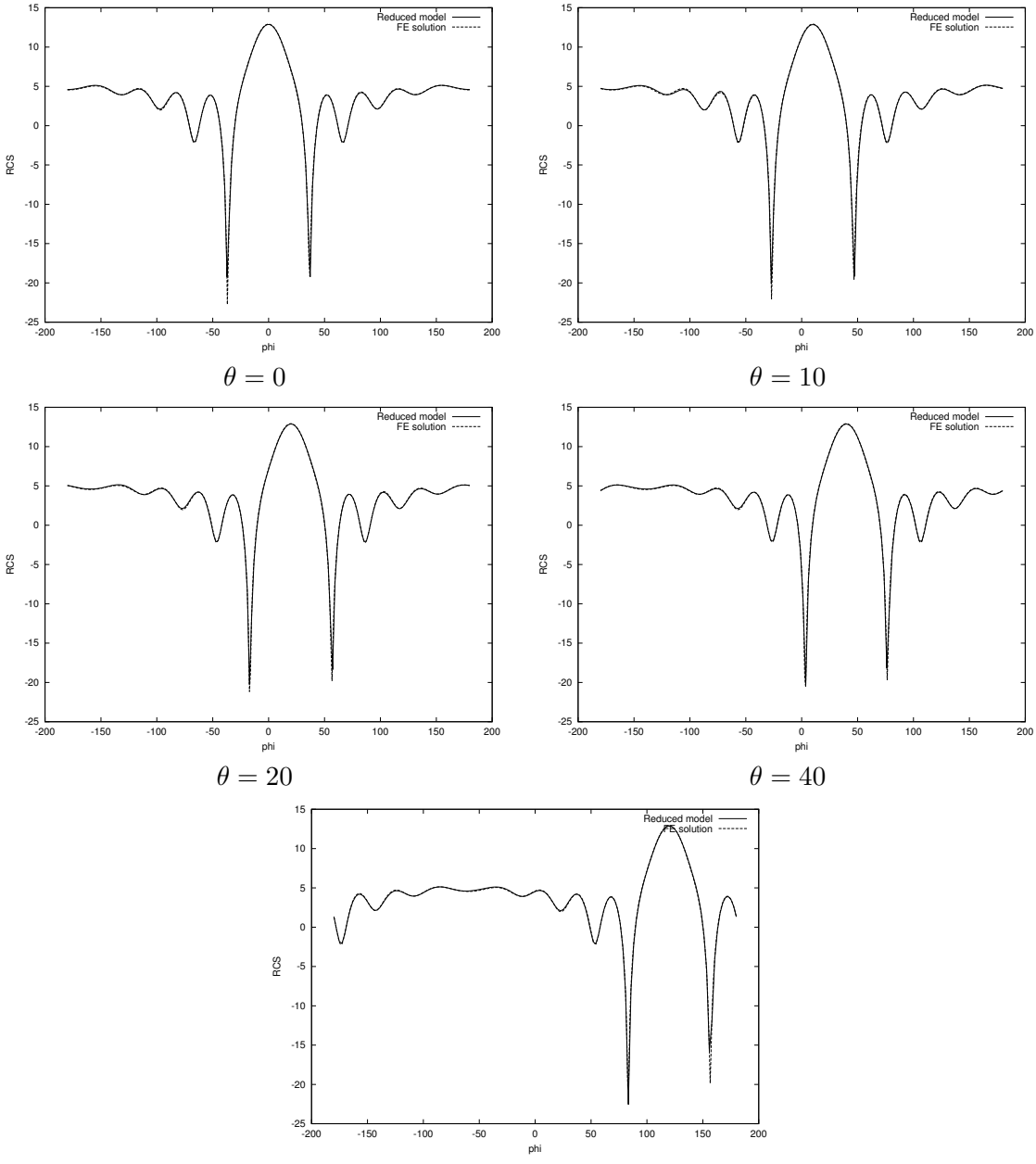

Figure 4: *Scattering of a plane TE wave by a PEC circular cylinder of diameter $D = 2\lambda$ showing a comparison between the scattering width distributions computed using the adjoint enhanced reduced–order model solution and the finite element solution, for waves incident at different angles, θ.*

$\theta = \{10, 20, 40, 120\}$, which do not correspond to one of the primal problems, the reduced–order approximation is in excellent agreement with the output given by the corresponding full finite element solution.

In Figure 4, the corresponding results for the scattering of a TE wave by a PEC circular cylinder of diameter $D = 2\lambda$ are displayed. For this example, we employ the same mesh and compute $N_\theta = 3$ scattering solutions and $N_\phi = 18$ adjoint solutions. As in the PMC case, it is observed that the scattering width distributions produced by the reduced–order approximation are again in excellent agreement with those obtained from the full finite element solution.

As an example of a problem involving a more complicated geometry, the calculation of the scattering width distribution for the problem of scattering of a plane TE wave by PEC NACA0012 aerofoil of electrical length 2λ is considered. The hybrid mesh that is employed is illustrated in

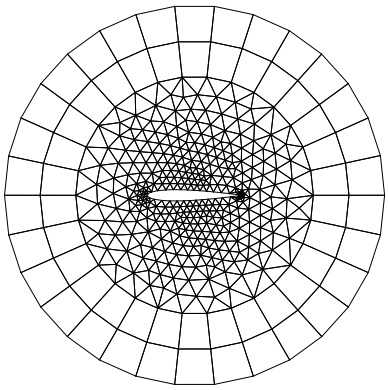

Figure 5: *Scattering by a PEC NACA0012 aerofoil of chord length* 2λ *showing the hybrid mesh of* 668 *triangles and* 60 *quadrilaterals.*

Figure 5 and contains 668 triangles and 60 quadrilaterals with uniform polynomial order $p = 3$. Off–line calculations are undertaken with $N_\theta = 3$ and $N_\phi = 18$. The reduced–order model scattering width distributions, for incident wave directions $\theta = \{0, 10, 20, 40, 120\}$, are compared with the distributions computed from the full finite element solution in Figure 6. It can be seen that excellent agreement is again obtained.

5.2 Bounds for the Reduced Order Approximation

To obtain tight bounds, it has been found to be necessary to increase the number of incident directions employed for the off–line computations [2]. However, this poor effectivity is offset by the fact that certainty of the solution is obtained and that the reduced order model computations are cheap. To illustrate this, consider again the case of scattering of a plane TE wave by a PMC circular cylinder of diameter $D = 2\lambda$, but now involving off–line computations for $N_\theta = 20$, with $\theta_i = -180+18(i-1)$ degrees, $i = 1, \cdots, 20$, and $N_\phi = 20$, with $\phi_i = -180+18(i-1)$, $i = 1, \cdots, 20$. In Figure 7, we show the corresponding upper and lower certainty bounds for the scattering width distributions which are obtained for on–line solutions with incident wave directions $\theta = 0, 10, 20, 40, 120$ degrees. It may be observed that the bound gap vanishes completely for $\theta = 0$, as this angle represents one of the values of θ_i for the primal problem. At other incident directions, we see that the bound gap vanishes at locations of ϕ corresponding to one of the values of ϕ_i for the dual problem. The magnitude of the certainty bounds for an on–line solution at an incident wave direction of $\theta = 20$ are smaller than those obtained for an on–line solution with an incident wave direction of $\theta = 10$. This is because the incident wave direction $\theta = 10$ degrees lies further away from the incident wave directions that were selected for the primal problem. Increasing N_θ and N_ϕ has the effect of reducing the magnitude of the bound gap.

[2]The size of the bound gap depends on the product of the norms of the residuals for the primal and dual problems. Therefore, to obtain tight bounds one must make this product sufficiently small. This can be achieved by increasing either N_θ or N_ϕ. However, we believe it is more computationally advantages to have $N_\theta \approx N_\phi$

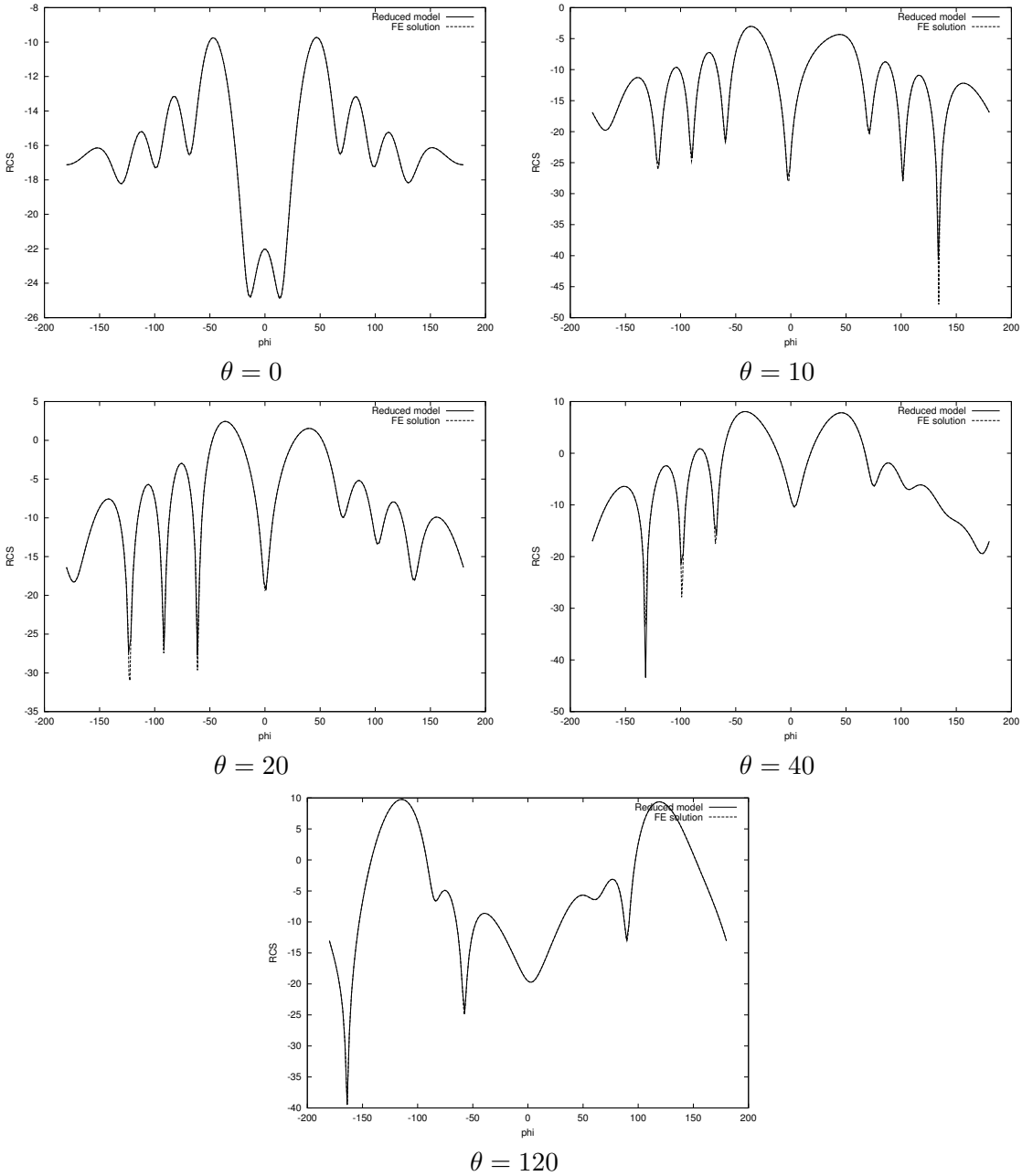

Figure 6: *Scattering of a plane TE wave by a PEC NACA0012 of electrical length* 2λ *showing a comparison between the scattering width distributions computed using the adjoint enhanced reduced–order model solution and the finite element solution, for waves incident at different angles,* θ*.*

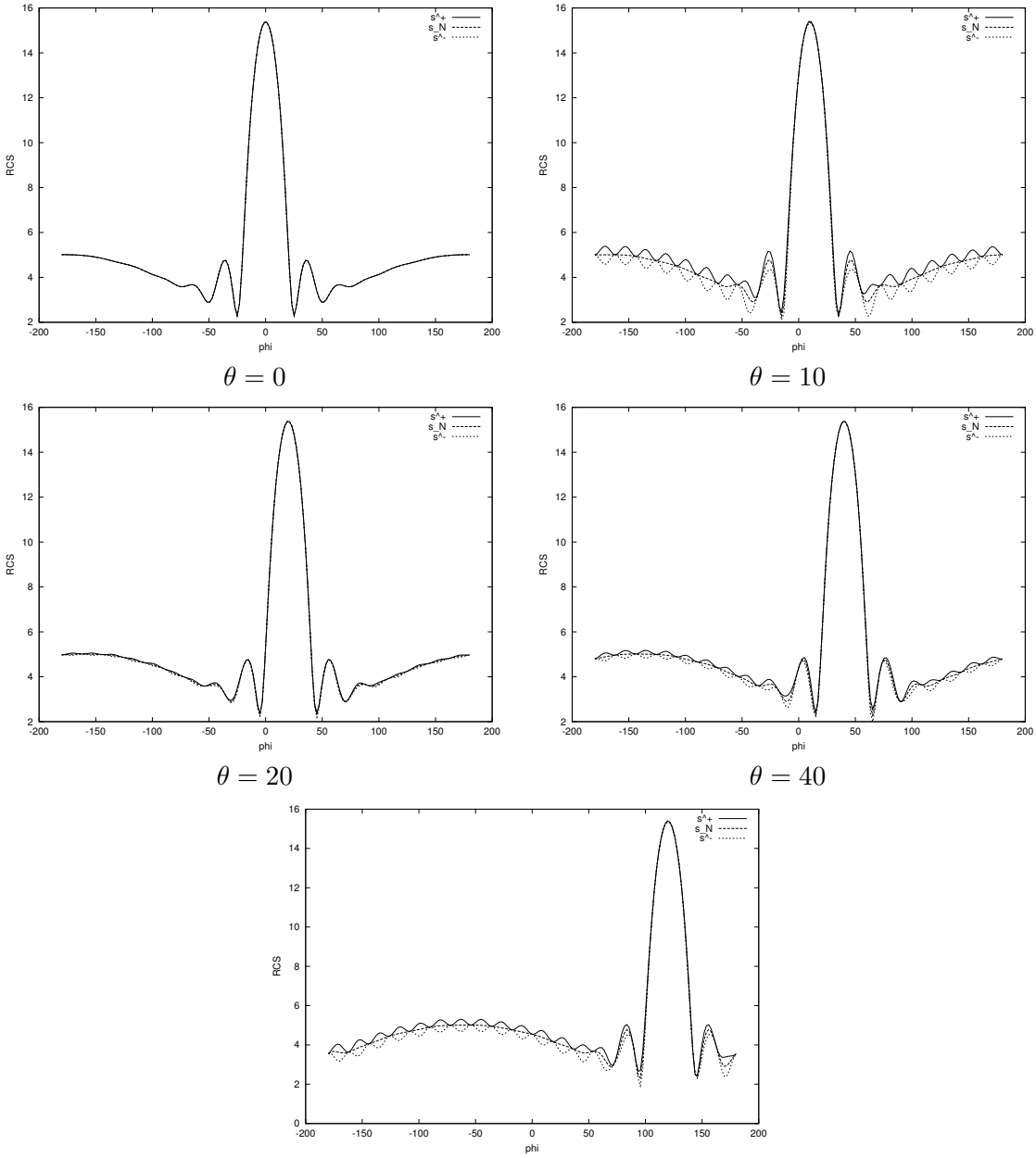

Figure 7: *Scattering of a plane TE wave by a PMC cylinder of electrical length* 2λ *showing the upper and lower certainty bounds and the predicted scattering width distributions for the reduced–order model at different angles,* θ*.*

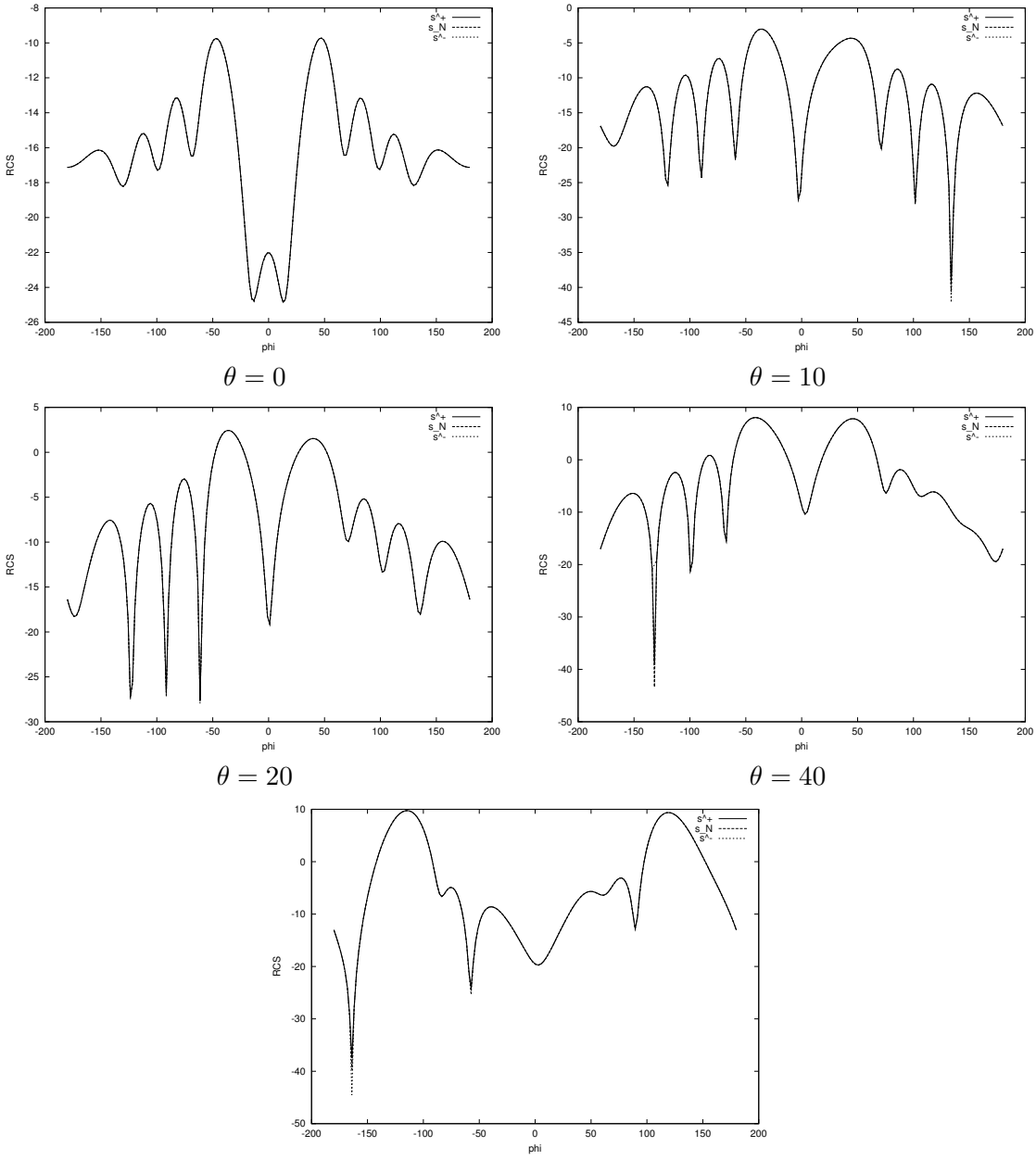

Figure 8: *Scattering of a plane TE wave by a PEC NACA0012 aerofoil of electrical length* 2λ *showing the upper and lower certainty bounds and the predicted scattering width distributions for the reduced–order model at different angles,* θ*.*

The minimum singular value for the matrix **A** for this problem was found to be approximately 1.12, which is close to unity. This means that the magnitude of the bounds are effectively governed by the Euclidean norms of the residuals.

To complete this section, we illustrate the computation of bounds for the problem of scattering of a plane TE wave by a PEC NACA0012 aerofoil of electrical length 2λ. In this case, for the off–line computations we take $N_\theta = 19$ scattering solutions, with incident directions $\theta_i = -180 + (360/19)(i-1)$ degrees for $i = 1, \cdots, 19$, and $N_\phi = 19$ adjoint solutions, with viewing angles $\phi_i = -180 + (360/19)(i-1)$ degrees for $i = 1, \cdots, 19$. The corresponding upper and lower bounds for the scattering width distributions which are obtained for on–line solutions with $\theta = 0, 10, 20, 40, 120$ degrees are displayed in Figure 8. It can be observed that the upper and lower bounds are very tight and almost indistinguishable from the distribution predicted by the reduced–order model.

Finally, in Figure 9 we examine the convergence of the maximum relative bound gap for increasing values of N_θ and N_ϕ. For this, we consider the scattering of a TE wave by a PMC cylinder of diameter $D = 2\lambda$ and the RCS distributions at $\theta = \{10, 20, 40, 120\}$. We increase $N_\theta = N_\phi$ from 14 to 21, and determine the maximum of the relative bound gap in each case. We observe, that for all values of θ considered, the trend is an exponential type convergence with increasing $N_\theta = N_\phi$. Note that for the case of $N_\theta = N_\phi = 18$ and the angles $\theta = \{20, 40, 120\}$ the bound gap vanishes and the reduced-order prediction coincides with the finite element solution, hence no point on the graph is given.

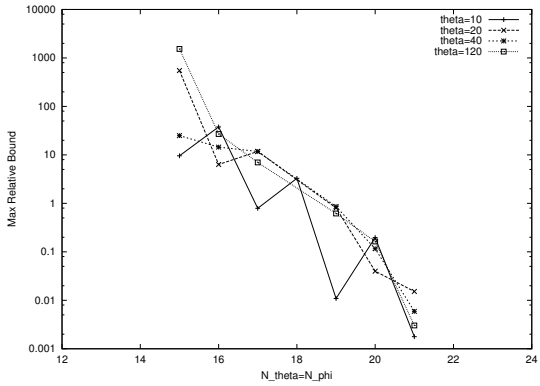

Figure 9: *Scattering of a plane TE wave by a PMC cylinder of electrical length* 2λ *showing the convergence of the maximum relative bound gap for the reduced–order model at different angles,* θ *and different values of* $N_\theta = N_\phi$.

6 Conclusions

In this paper, a reduced–order approximation for the rapid calculation of scattering width distributions in two dimensional electromagnetic wave scattering problems has been proposed. The method has been shown to produce accurate scattering width distributions for new incident wave directions, using data from only a small number of off–line solutions. A novel method for obtaining tight bounds on the distribution predicted by the reduced–order approximation has also been described. Work is currently in progress to extend this approach to include varying frequency and changes in geometry.

Acknowledgements

Paul Ledger acknowledges the support of the UK Engineering and Physical Sciences Research Council (EPSRC) in the form of a PhD studentship under grant GR/M59112. Jaime Peraire

acknowledges the support of EPSRC in the form of a visiting fellowship award under grant GR/N09084.

References

[1] Kirsch A. *An Introduction to the Mathematical Theory of Inverse Problems*, Springer–Verlag 1996.

[2] Wilcox KE, Paduano JD, Peraire J. Low order aerodynamic models for areoelastic control of turbomachines. in *40th Structures, Structural Dynamics and Materials Conference*, AIAA 99–1467, St–Louis, 1999.

[3] Wilcox KE, Peraire J, White J. An Arnoldi approach for generation of reduced–order models for turbomachinery. Submitted to Computers and Fluids, 1999.

[4] Machiels L, Maday Y, Patera AT. Output bounds for reduced–order approximations of elliptic partial differential equations. *Computer Methods in Applied Mechanics and Engineering* 2001; **190**: 3413-3426.

[5] Maday Y, Patera AT, Rovas DV. A black box reduced–basis output bound method for non–coercive problems. in *Non–linear Partial Differential Equations and their Applications*. Proceedings of the College De France Seminars, 2001.

[6] Ainsworth M, Coyle J. Hierarchic *hp*–edge element families for Maxwell's equations in hybrid quadrilateral/triangular meshes. *Computer Methods in Applied Mechanics and Engineering* 2001; **190**:6709–6733.

[7] Ledger PD, Morgan K, Hassan O, Weatherill NP. Arbitrary order edge elements for electromagnetic scattering simulations using hybrid meshes and a PML. *International Journal for Numerical Methods in Engineering* 2002;**55**:339–358.

[8] Ledger PD. *An hp–Adaptive Finite Element Procedure for Electromagnetic Scattering Problems* PhD Thesis University of Wales, Swansea, 2001.

[9] Cecot W, Demkowicz L, Rachowicz W. A two-dimensional infinite element for Maxwell's equations. *Computer Methods in Applied Mechanics and Engineering* 2000;**188**:625–643.

[10] Bettess P. *Infinite Elements*, Penshaw Press, Sunderland 1992.

[11] Bayliss A, Turkel E. Radiation boundary conditions for wave–like equations. *Communications in Pure and Applied Mathematics* 1980;**33**: 707–725.

[12] Givoli D. Recent advances in the DtN FE Method. *Archives of Computational Methods in Engineering* 1999;**6**:71–116.

[13] Jin J–M, Volakis JL, Collins JD. A finite element–boundary integral method for scattering and radiation by two– and three–dimensional structures. *IEEE Antennas and Propagation Magazine* 1991; **33**:22–32.

[14] Berenger J–P. A perfectly matched layer for the absorption of electromagnetic waves. *Journal of Computational Physics* 1994; **114**: 185–200.

[15] Kuzuoglu M, Mittra R. Investigation of non-planar perfectly matched absorber for finite element mesh truncation. *IEEE Transactions on Antennas and Propagation* 1997; **45**: 474–486.

[16] Demkowicz L, Vardapetyan L. Modelling of electromagnetic absorption/scattering problems using *hp*-adaptive finite elements. *Computer Methods in Applied Mechanics and Engineering* 1998 **152**: 103–124.

[17] Stratton JA. *Electromagnetic Theory*, McGraw–Hill, New York, 1941.

[18] Ledger PD, Morgan K, Peraire J, Hassan O, Weatherill NP. Efficient, highly accurate *hp*–adaptive finite element computations of the scattering width output of Maxwell's equations Submitted to *International Journal for Numerical Methods in Fluids*, 2002.

[19] Monk P. The near to far field transformation. *International Journal for Computation and Mathematics in Electrical and Electronic Engineering* 1995;**14**:41–56.

[20] Monk P, Suli E. The adaptive computation of far field patterns by a–posteriori error estimation of linear functionals. *SIAM Journal of Numerical Analysis* 1998;**36**: 251–274.

[21] Monk P, Parott K. Phase accuracy and improved farfield estimates for 3–D edge elements on tetrahedral meshes. *Journal of Computational Physics* 2001;**170**:614-641.